Measurement of charm production cross sections in e^+e^- annihilation at energies between 3.97 and 4.26 GeV

D. Cronin-Hennessy,[1] K. Y. Gao,[1] J. Hietala,[1] Y. Kubota,[1] T. Klein,[1] B. W. Lang,[1] R. Poling,[1] A. W. Scott,[1] P. Zweber,[1] S. Dobbs,[2] Z. Metreveli,[2] K. K. Seth,[2] A. Tomaradze,[2] J. Libby,[3] A. Powell,[3] G. Wilkinson,[3] K. M. Ecklund,[4] W. Love,[5] V. Savinov,[5] A. Lopez,[6] H. Mendez,[6] J. Ramirez,[6] J. Y. Ge,[7] D. H. Miller,[7] I. P. J. Shipsey,[7] B. Xin,[7] G. S. Adams,[8] M. Anderson,[8] J. P. Cummings,[8] I. Danko,[8] D. Hu,[8] B. Moziak,[8] J. Napolitano,[8] Q. He,[9] J. Insler,[9] H. Muramatsu,[9] C. S. Park,[9] E. H. Thorndike,[9] F. Yang,[9] M. Artuso,[10] S. Blusk,[10] S. Khalil,[10] J. Li,[10] R. Mountain,[10] S. Nisar,[10] K. Randrianarivony,[10] N. Sultana,[10] T. Skwarnicki,[10] S. Stone,[10] J. C. Wang,[10] L. M. Zhang,[10] G. Bonvicini,[11] D. Cinabro,[11] M. Dubrovin,[11] A. Lincoln,[11] J. Rademacker,[12] D. M. Asner,[13] K. W. Edwards,[13] P. Naik,[13] J. Reed,[13] R. A. Briere,[14] T. Ferguson,[14] G. Tatishvili,[14] H. Vogel,[14] M. E. Watkins,[14] J. L. Rosner,[15] J. P. Alexander,[16] D. G. Cassel,[16] J. E. Duboscq,[16] R. Ehrlich,[16] L. Fields,[16] L. Gibbons,[16] R. Gray,[16] S. W. Gray,[16] D. L. Hartill,[16] B. K. Heltsley,[16] D. Hertz,[16] C. D. Jones,[16] J. Kandaswamy,[16] D. L. Kreinick,[16] V. E. Kuznetsov,[16] H. Mahlke-Krüger,[16] D. Mohapatra,[16] P. U. E. Onyisi,[16] J. R. Patterson,[16] D. Peterson,[16] D. Riley,[16] A. Ryd,[16] A. J. Sadoff,[16] X. Shi,[16] S. Stroiney,[16] W. M. Sun,[16] T. Wilksen,[16] S. B. Athar,[17] R. Patel,[17] J. Yelton,[17] P. Rubin,[18] B. I. Eisenstein,[19] I. Karliner,[19] S. Mehrabyan,[19] N. Lowrey,[19] M. Selen,[19] E. J. White,[19] J. Wiss,[19] R. E. Mitchell,[20] M. R. Shepherd,[20] D. Besson,[21] and T. K. Pedlar[22]

(CLEO Collaboration)

[1]*University of Minnesota, Minneapolis, Minnesota 55455, USA*
[2]*Northwestern University, Evanston, Illinois 60208, USA*
[3]*University of Oxford, Oxford OX1 3RH, United Kingdom*
[4]*State University of New York at Buffalo, Buffalo, New York 14260, USA*
[5]*University of Pittsburgh, Pittsburgh, Pennsylvania 15260, USA*
[6]*University of Puerto Rico, Mayaguez, Puerto Rico 00681*
[7]*Purdue University, West Lafayette, Indiana 47907, USA*
[8]*Rensselaer Polytechnic Institute, Troy, New York 12180, USA*
[9]*University of Rochester, Rochester, New York 14627, USA*
[10]*Syracuse University, Syracuse, New York 13244, USA*
[11]*Wayne State University, Detroit, Michigan 48202, USA*
[12]*University of Bristol, Bristol BS8 1TL, United Kingdom*
[13]*Carleton University, Ottawa, Ontario, Canada K1S 5B6*
[14]*Carnegie Mellon University, Pittsburgh, Pennsylvania 15213, USA*
[15]*Enrico Fermi Institute, University of Chicago, Chicago, Illinois 60637, USA*
[16]*Cornell University, Ithaca, New York 14853, USA*
[17]*University of Florida, Gainesville, Florida 32611, USA*
[18]*George Mason University, Fairfax, Virginia 22030, USA*
[19]*University of Illinois, Urbana-Champaign, Illinois 61801, USA*
[20]*Indiana University, Bloomington, Indiana 47405, USA*
[21]*University of Kansas, Lawrence, Kansas 66045, USA*
[22]*Luther College, Decorah, Iowa 52101, USA*

(Received 20 January 2008; published 1 October 2009)

Using the CLEO-c detector at the Cornell Electron Storage Ring, we have measured inclusive and exclusive cross sections for the production of D^+, D^0 and D_s^+ mesons in e^+e^- annihilations at 13 center-of-mass energies between 3.97 and 4.26 GeV. Exclusive cross sections are presented for final states consisting of two charm mesons ($D\bar{D}$, $D^*\bar{D}$, $D^*\bar{D}^*$, $D_s^+D_s^-$, $D_s^{*+}D_s^-$, and $D_s^{*+}D_s^{*-}$) and for processes in which the charm-meson pair is accompanied by a pion. No enhancement in any final state is observed at the energy of the $Y(4260)$.

DOI: 10.1103/PhysRevD.80.072001 PACS numbers: 13.66.Bc, 13.25.Gv

I. INTRODUCTION

Hadron production in electron-positron annihilations just above $c\bar{c}$ threshold has been a subject of mystery and little intensive study for more than three decades since the discovery of charm. Recent developments, like the observation of the $Y(4260)$ reported by the *BABAR* Collaboration [1] and subsequently confirmed by CLEO-c [2] and Belle [3], underscore our incomplete understand-

ing and demonstrate the potential for discovery of new states, such as hybrids and glueballs. It is also clear that precise measurements of charm-meson properties will shed light on higher-energy investigations of b-flavored particles and new states that might decay into b. Charm decays also offer unique opportunities to test the validity and guide the development of theoretical tools, like lattice QCD, that are needed to interpret measurements of the quark-mixing parameters described by the Cabibbo-Kobayashi-Maskawa matrix [4]. Any comprehensive program of precise charm-decay measurements demands a detailed understanding of charm production.

Most past studies of hadron production in the charm-threshold region have been measurements of the ratio $R(s) = \sigma(e^+e^- \to \text{hadrons})/\sigma(e^+e^- \to \mu^+\mu^-)$ over this energy range that have been made by many experiments [5]. Recent measurements with the Beijing Spectrometer (BES) [6] near charm threshold are especially noteworthy. There is a rich structure in this energy region, reflecting the production of $c\bar{c}$ resonances and the crossing of thresholds for specific charm-meson final states. Interesting features in the hadronic cross section between 3.9 and 4.2 GeV include a large enhancement at the threshold for $D^*\bar{D}^*$ production (4.02 GeV) and a fairly large plateau that begins at $D_s^{*+}D_s^-$ threshold (4.08 GeV). While there is considerable theoretical interest [7–10], there has been little experimental information about the composition of these enhancements.

In this paper we describe measurements of charm-meson production in e^+e^- annihilations at 13 center-of-mass energies between 3970 and 4260 MeV. These studies were carried out with the CLEO-c detector at the Cornell Electron Storage Ring (CESR) [11] in 2005–2006. (Throughout this paper use of any particular mode implies use of the charge-conjugate mode as well.) The principal objective of the CLEO-c energy scan was to determine the optimal running point for studies of D_s^+-meson decays. The same data sample has been used to confirm the direct production of $Y(4260)$ in e^+e^- annihilations and to demonstrate $Y(4260)$ decays to final states in addition to $\pi^+\pi^- J/\psi$ [2]. Specific results presented in this paper include cross-section measurements for exclusive final states with D^+, D^0 and D_s^+ mesons and inclusive measurements of the total charm-production cross section and $R(s)$.

II. DATA SAMPLE AND DETECTOR

The data sample for this analysis was collected with the CLEO-c detector. Both the fast-feedback analysis carried out as data were collected and the detailed analysis reported here are extensions of techniques developed for charm-meson studies at the $\psi(3770)$ [12].

An initial energy scan, conducted during August–October, 2005, consisted of 12 energy points between 3970 and 4260 MeV, with a total integrated luminosity of 60.0 pb^{-1}. The scan was designed to provide cross-section measurements at each energy for all accessible final states consisting of a pair of charm mesons. At the highest energy point these include $D\bar{D}$, $D^*\bar{D}$, $D^*\bar{D}^*$, $D_s^+D_s^-$, $D_s^{*+}D_s^-$, and $D_s^{*+}D_s^{*-}$, where the first three include both charged and neutral mesons. A follow-up run beginning early in 2006 provided a larger sample of 178.9 pb^{-1} at 4170 MeV, not one of the original scan points, that proved essential in understanding the composition of charm production throughout this energy region.

The center-of-mass energies and integrated luminosities for the 13 subsamples are listed in Table I. Integrated luminosity is determined by measuring the processes $e^+e^- \to e^+e^-$, $\mu^+\mu^-$, and $\gamma\gamma$ [13], which are used because their cross sections are precisely determined by QED. Each of the three final states relies on different components of the detector, with different systematic effects. The three individual results are combined using a weighted average to obtain the luminosity used for this analysis.

CLEO-c is a general-purpose magnetic spectrometer with most components inherited from the CLEO III detector [14], which was constructed primarily to study B decays at the $\Upsilon(4S)$. Its cylindrical charged-particle tracking system covers 93% of the full 4π solid angle and consists of a six-layer all-stereo inner drift chamber and a 47-layer main drift chamber. These chambers are coaxial with a superconducting solenoid that provides a uniform 1.0-T magnetic field throughout the volume occupied by all active detector components used for this analysis. Charged particles are required to satisfy criteria ensuring successful fits and vertices consistent with the e^+e^- collision point. The resulting momentum resolution is $\sim$0.6% at 1 GeV/c for tracks that traverse all layers of the drift chamber. Oppositely charged and vertex-constrained pairs of tracks are identified as $K_S^0 \to \pi^+\pi^-$ candidates if their invariant mass is within 4.5 standard deviations (σ) of the known mass ($\sim$ 12 MeV/c^2).

TABLE I. Center-of-mass energies and integrated luminosity totals for all data samples used in this paper.

$E_{\text{c.m.}}$ (MeV)	$\int \mathcal{L}dt$ (pb^{-1})
3970	3.85
3990	3.36
4010	5.63
4015	1.47
4030	3.01
4060	3.29
4120	2.76
4140	4.87
4160	10.16
4170	178.89
4180	5.67
4200	2.81
4260	13.11

TABLE II. The decay modes used to determine the D_s cross sections, with branching fractions ($\mathcal{B}$) and references.

Modes	Reference	$\mathcal{B}$ (%)
$K^+K^-\pi^+$, $\lvert M_{KK} - M_\phi\rvert < (10\ \mathrm{MeV}/c^2)$	[15]	1.99 ± 0.11
$\bar{K}^{*0}K^+$, $\bar{K}^{*0} \to K^-\pi^+$	[5]	2.2 ± 0.6
$\eta\pi^+$, $\eta \to \gamma\gamma$	[5,15]	0.62 ± 0.08
$\eta\rho^+$, $\eta \to \gamma\gamma$, $\rho^+ \to \pi^+\pi^0$	[5]	4.3 ± 1.2
$\eta'\pi^+$, $\eta' \to \pi^+\pi^-\eta$, $\eta \to \gamma\gamma$	[5,15]	0.66 ± 0.07
$\eta'\rho^+$, $\eta' \to \pi^+\pi^-\eta$, $\eta \to \gamma\gamma$, $\rho^+ \to \pi^+\pi^0$	[5]	1.8 ± 0.5
$\phi\rho^+$, $\phi \to K^+K^-$, $\rho^+ \to \pi^+\pi^0$	[5]	3.4 ± 1.2
$K_S K^+$, $K_S \to \pi^+\pi^-$	[5,15]	1.03 ± 0.06

The main drift chamber also provides dE/dx measurements for charged-hadron identification, complemented by a Ring-Imaging Cherenkov (RICH) detector covering 80% of 4π. The rate of pions faking kaons is $(1.10 \pm 0.37)\%$, with a pion identification efficiency for tracks in the RICH of $(94.5 \pm 0.4)\%$. The rate of kaons faking pions is $(2.47 \pm 0.38)\%$, with a kaon identification efficiency for tracks in the RICH of $(88.4 \pm 0.6)\%$.

An electromagnetic calorimeter constructed of 7784 CsI(Tl) crystals provides electron identification and neutral detection over 93% of 4π, with photon-energy resolution of 2.2% at 1 GeV and 5% at 100 MeV. We select π^0 and η candidates from pairs of photons with invariant masses within 3σ of the known values [5] ($\sigma \sim 6\ \mathrm{MeV}/c^2$ for π^0 and $\sigma \sim 12\ \mathrm{MeV}/c^2$ for η).

III. EVENT-SELECTION PROCEDURES

The procedures and specific criteria for the selection of D^+, D^0 and D_s^+ mesons closely follow previous CLEO-c analyses and are described in Refs. [12,15]. Candidates are identified based on their invariant masses and total energies, with selection criteria optimized on a mode-by-mode basis. We use only the cleanest final states for D^0 ($K^-\pi^+$) and D^+ ($K^-\pi^+\pi^+$) selection, since these provide sufficient statistics for precise cross-section determinations. For D_s^+ we optimize for efficiency by selecting the eight decay modes listed in Table II. Accepted intermediate-particle decay modes (mass cuts) are $\phi \to K^+K^-$ (± 10 MeV), $\bar{K}^{*0} \to K^-\pi^+$ (± 75 MeV), $\eta' \to \eta\pi^+\pi^-$ (± 10 MeV), and $\rho^+ \to \pi^+\pi^0$ (± 150 MeV).

To determine the production yields and cross sections for the final states accessible at a particular center-of-mass energy, we classify events based on the energy and momentum of $D_{(s)}$ candidate in the form of the energy difference ($\Delta E \equiv E_{D_{(s)}} - E_{\mathrm{beam}}$) and beam-constrained mass ($M_{\mathrm{bc}} \equiv \sqrt{E_{\mathrm{beam}}^2 - |\mathbf{P}_{D_{(s)}}|^2}$), where $E_{D_{(s)}}$ and $p_{D_{(s)}}$ are the energy and three-momentum of the $D_{(s)}$ candidate. Figure 1 shows the expected behavior of D^0 candidates in a Monte Carlo study of CLEO-c data at a center-of-mass energy of 4160 MeV in a two-dimensional plot of ΔE vs M_{bc}. The Monte Carlo sample represents about 10 times the integrated luminosity that was collected at that energy. The contributions of the accessible final states consisting of two charm mesons are evident and demarcated by the ellipses drawn on the figure. This separation was exploited during the scan running for a fast-feedback "cut-and-count" determination of event yields. The task was to count events consistent with production through specific modes, and determine cross sections after accounting for backgrounds and cross feed from other modes. The separation is cleanest for D^0 mesons produced in $D\bar{D}$ events, for which the only contributing process is $D^0\bar{D}^0$. For D^0's produced in $D^*\bar{D}$ and $D^*\bar{D}^*$ events, the situation is complicated and the separation reduced by contributions from both $D^{*0} \to D^0\pi^0$ or $D^0\gamma$ and $D^{*+} \to D^0\pi^+$.

The same separation is also evident in plots of the momenta of charm-meson candidates selected by cutting on the candidate invariant mass. Figure 2 illustrates this with the momentum spectra for $D^0 \to K^-\pi^+$ candidates within 15 MeV of the nominal mass both in the Monte Carlo sample of Fig. 1 and in 10.16 pb^{-1} of CLEO-c data at 4160 MeV. While no background correc-

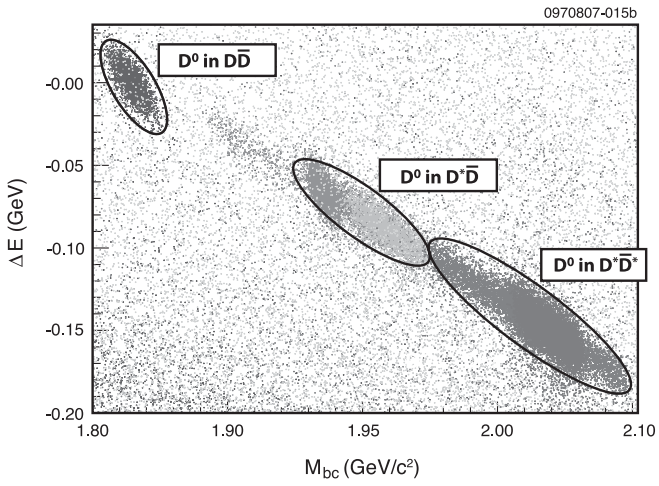

FIG. 1. ΔE vs M_{bc} for $D^0 \to K^-\pi^+$ candidates in a Monte Carlo simulation of CLEO-c data at a center-of-mass energy of 4160 MeV. Separation among the expected two-charm-meson final states is evident, as described in the text.

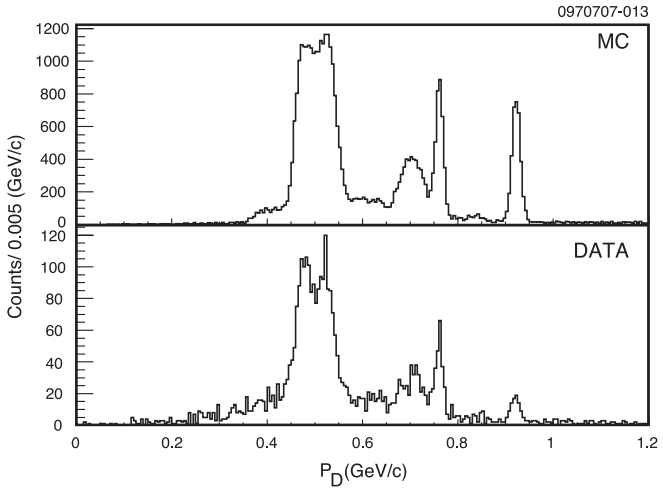

FIG. 2. Momentum spectra in Monte Carlo simulation (top) and data (bottom) at 4160 MeV for $D^0 \to K^-\pi^+$ candidates with invariant masses within 15 MeV of the nominal value. There is reasonable agreement between the Monte Carlo simulation and data, with clear peaks corresponding to the expected final states with two charm mesons at this energy ($D\bar{D}$, $D^*\bar{D}$ and $D^*\bar{D}^*$). Quantitative interpretation of the momentum spectrum requires correction for non-charm-meson backgrounds, consideration of additional channels for charm-meson production, radiative effects, and other phenomena, as described in the text.

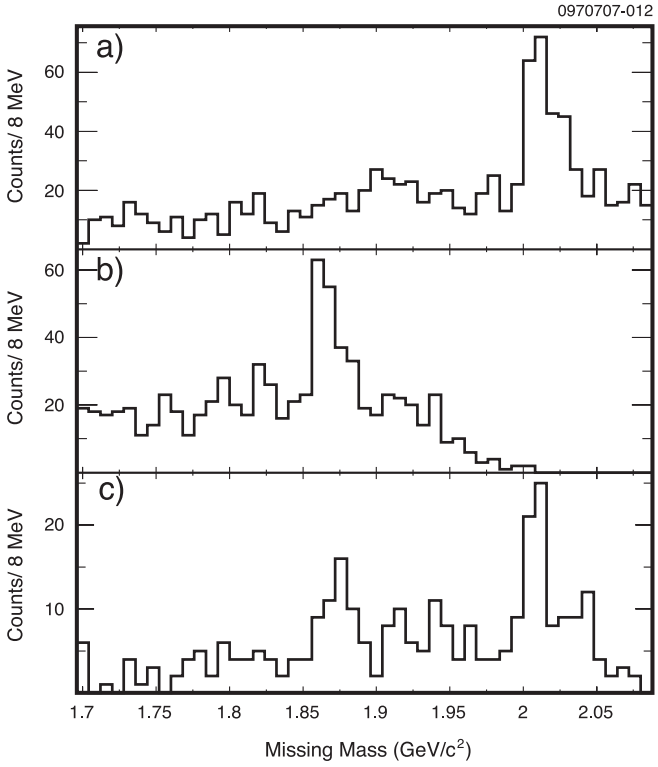

FIG. 3. The mass spectrum of X in (a) $e^+e^- \to D^0\pi^\pm X$ at 4170 MeV, (b) $e^+e^- \to D^{*\pm}\pi^\mp X$ at 4170 MeV, and (c) $e^+e^- \to D^{*0}\pi^\pm X$ at 4260 MeV. Peaks at the D^* mass in (a) and the D mass in (b) are evidence for the decay $D^*\bar{D}\pi$. The D peak in (c) confirms $D^*\bar{D}\pi$ and the D^* peak demonstrates that $D^*\bar{D}^*\pi$ is produced at 4260 MeV.

tions have been applied to these distributions, the structure of distinct Doppler-smeared peaks corresponding to different final states is evident. The Monte Carlo prediction and data show good qualitative agreement, with concentrations of events corresponding to prominent final states near 0.95 GeV/c ($D\bar{D}$), 0.73 GeV/c ($D^*\bar{D}$) and 0.5 GeV/c ($D^*\bar{D}^*$). This illustrates that the composition of final states can also be determined by fitting the momentum spectra of D^0, D^+ and D_s^+ candidates.

The cross sections for all contributing final states can be determined by correcting the raw measured momentum spectra like Fig. 2 for combinatoric and other backgrounds and then fitting to Monte Carlo predictions of the spectra. To achieve good fits, all significant production mechanisms must be included and the predicted spectra must reflect correct D^*-decay angular distributions and the effects of initial state radiation (ISR).

IV. EVIDENCE FOR MULTIBODY PRODUCTION

While the qualitative features of the measured charm-meson momentum spectra accorded with expectations (Fig. 2), initial attempts to fit the spectra did not produce acceptable results. It was quickly concluded that the two-body processes listed above are insufficient to account for all observed charm-meson production. Final states like $D\bar{D}^{(*)}\pi(\pi\ldots)$, in which the charm-meson pair is accompanied by one or more additional pions, emerged as a likely explanation. While not unexpected, these ''multibody'' events have not previously been observed in the charm-threshold region, and there are no predictions of the cross sections for D^0 and D^+ production through multibody final states.

To assess which multibody final states ($D\bar{D}\pi$, $D^*\bar{D}\pi$, etc.) are measurably populated in our data, we examine observables other than the charm-meson momenta, because ISR causes smearing of the peaks in the momentum spectra that can obscure the two-body kinematics. We applied $D^{(*)}$ momentum selection criteria to exclude two-body contributions and examined the distributions of missing mass against a $D^{(*)}$ and an accompanying charged or neutral pion, using charge correlations to suppress incorrect combinations. Figure 3 shows clear evidence for $D^*\bar{D}\pi$ events at 4170 MeV, as well as indications of $D^*\bar{D}^*\pi$ in the sample of 13 pb^{-1} collected at 4260 MeV [Fig. 3(c)]. These events cannot be attributed to two-body production with ISR, because radiative photons would destroy any peaking in the missing-mass spectrum. The absence of a peak at the D mass in Fig. 3(a) indicates that there is no evidence for $D\bar{D}\pi$ production. Analysis of events with D_s reveals no evidence for multibody production, consistent with expectations, since the $D_s^+D_s^-\pi^0$ final state violates isospin conservation.

V. MOMENTUM-SPECTRUM FITS AND CROSS-SECTION RESULTS

Momentum spectra for D^0, D^+ and D_s^+ candidates were found by requiring the invariant mass of $D_{(s)}$ decay products to be within ± 15 MeV of the nominal value. Backgrounds are estimated with a sideband technique. Sideband regions are taken on both sides of the expected signal, and are significantly larger than the signal region to minimize statistical uncertainty in the background subtraction. Sideband widths are set mode by mode based on expectations for specific background processes.

Having identified the components of multibody charm production, we determine yields for these channels and the two-body modes by fitting the sideband-subtracted D^0, D^+ and D_s^+ momentum spectra. Signal momentum distributions for specific channels are based on full GEANT [16] simulations using EVTGEN [17] for the production and decay of charm mesons. The EVTGEN simulation incorporates all angular correlations by using individual amplitudes for each node in the decay chain. ISR is included in the simulation, which requires input of energy-dependent cross sections for each final state. We used simple parametrizations of these cross sections constructed by linearly interpolating between the preliminary measurements from our analysis. (In doing this we made the assumption that the energy dependence of the Born-level cross sections is adequately represented by the uncorrected cross sections.) For the multibody $D^*\bar{D}\pi$ and $D^*\bar{D}^*\pi$ final states we used a spin-averaged phase-space model within EVTGEN.

The momentum-dependent yields and fits to our large data sample at 4170 MeV are shown in Fig. 4. For the $D^0 \to K^-\pi^+$ fit [Fig. 4(a)], the data are shown as the points with errors and the total fit result is the black line. The contributions of specific production channels are shown as the colored lines, with normalizations determined by the fit. The narrow peak above 0.8 GeV/c (blue line) is D^0 from $D\bar{D}$. The structure near 0.7 GeV/c consists of $D^*\bar{D}$ events, including a sharp peak from the direct D^0 (red line), and smaller, broader, peaks just below from $D^{*+} \to D^0\pi^+$ (green line) and $D^{*0} \to D^0\pi^0$ (light blue line). The structure near 0.5 GeV/c includes all $D^*\bar{D}^*$ events, with the core from $D^{*+} \to D^0\pi^+$ (lavender line) and $D^{*0} \to D^0\pi^0$ (amber line), and the broader lower component from $D^{*0} \to D^0\gamma$ (yellow line). Multibody final states $D^*\bar{D}\pi$ (dark red line) are combined and are visible as the broad spectrum between 0 and 0.5 GeV/c. Each component was broken down for the fit into ISR and non-ISR components, with their relative normalizations free. They have been combined for display purposes. The fit reproduces all of the major features of the data, including the peaks, tails and resolutions. The quantitative fit quality (χ^2 of 248 for 132 degrees of freedom) verifies that there are no significant omissions in the exclusive contributions or major deficiencies in the detector simulation, but that some of the details of the modeling of the contributing processes do not precisely match the data.

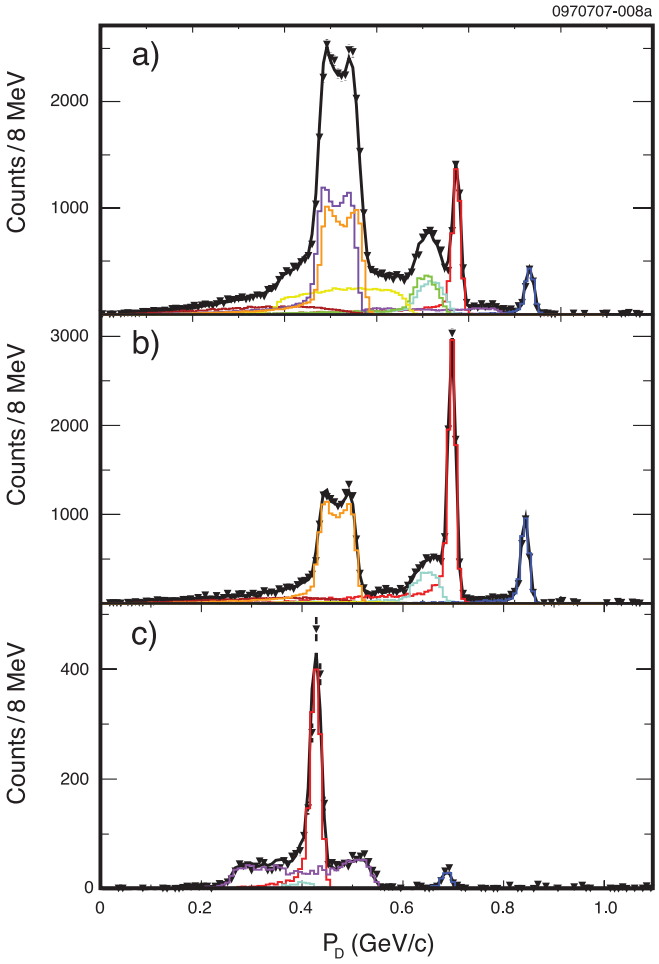

FIG. 4 (color). Sideband-subtracted momentum spectra for (a) $D^0 \to K^-\pi^+$, (b) $D^+ \to K^-\pi^+\pi^+$, and (c) $D_s^+ \to \phi\pi^+$ at 4170 MeV. Data are shown as points with errors and the total fit result is shown as the solid black line. The colored histograms represent specific $D_{(s)}$-production mechanisms, with shapes obtained from Monte Carlo simulations and normalizations determined by the fits. The color code for the components of the fits and the χ^2 values is given in the text.

The fit to the $D^+ \to K^-\pi^+\pi^+$ [Fig. 4(b)] is very similar in execution and display to $D^0 \to K^-\pi^+$, with all of the same components except that there is no D^+ production from D^{*0}. The quality of this fit is better, with a χ^2 of 182 for 132 degrees of freedom.

The $D_s^+ \to \phi\pi^+$ fit at 4170 MeV [Fig. 4(c)] is simpler, because of the absence of $D_s^{*+}D_s^{*-}$ production. Here the components are $D_s^+D_s^-$ (blue line) at about 0.7 GeV/c and a broad structure centered just above 0.4 GeV/c from $D_s^{*+}D_s^-$. The latter consist of a main peak from the primary D_s^+ (red line) and the lower plateau consisting mainly of $D_s^{*+} \to D_s^+\gamma$ (lavender line), with a smaller contribution from $D_s^{*+} \to D_s^+\pi^0$. The lack of D_s^+ entries below $\sim$200 MeV confirms that multibody D_s production is neg-

ligible. Because of the relative simplicity of D_s production, demonstrated by the $D_s^+ \to \phi\pi^+$ fits, and the limited statistics of the sample, we determine the final cross sections for $D_s^+ D_s^-$, $D_s^{*+} D_s^-$ and $D_s^{*+} D_s^{*-}$ by using a sideband-subtraction technique to count signal events in a region of the $M_{\rm bc}$-ΔE plane. The cross sections are then determined from a weighted sum of the yields for the eight D_s decay modes given in Table II, with weights minimizing the combined statistical and systematic uncertainties calculated from previously measured branching fractions and efficiencies determined with Monte Carlo simulations. The cut-and-count analysis gives results that are consistent with momentum fits. There is good agreement among the separately calculated cross sections for the different D_s decay modes.

After this procedure was refined and verified on our 4170 MeV data sample, it was applied to the other 12 subsamples. Detailed fit results are available in Ref. [18]. Figure 5 shows the D^0, D^+ and D_s fits for the data sample at 4260 MeV, which are of particular interest because the charm-production cross sections might provide insight to the nature of the $Y(4260)$ state. The fits at 4260 MeV behave similarly to those at lower energy, although a larger proportion of multibody decays is apparent.

Cross sections for the two-body and multibody final states are shown in Fig. 6. The uncertainties on the data points are statistical and systematic combined in quadrature. Reference [18] provides detailed descriptions of the systematic uncertainties of the cross-section determinations. Briefly, there are three sources of systematic uncertainty: determination of the efficiency of charm-meson

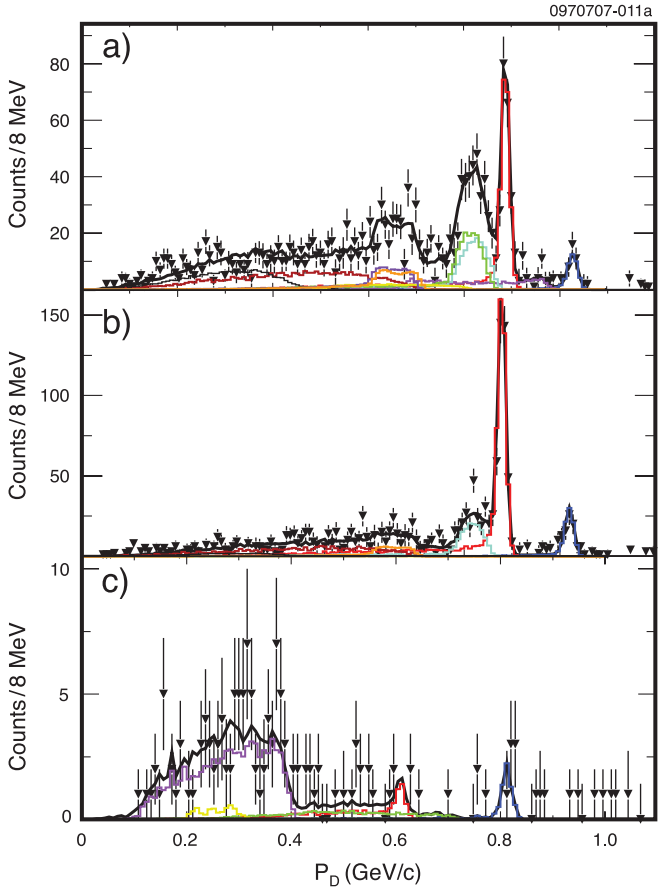

FIG. 5 (color). Sideband-subtracted momentum spectra for (a) $D^0 \to K^-\pi^+$, (b) $D^+ \to K^-\pi^+\pi^+$, and (c) $D_s^+ \to \phi\pi^+$ at 4260 MeV. Data are shown as points with errors and the total fit result is shown as the solid black line. The colored histograms represent specific $D_{(s)}$-production mechanisms, with shapes obtained from Monte Carlo simulations and normalizations determined by the fits. The color coding for the components matches that of Fig. 4, as described in the text. All peaks are shifted slightly higher in momentum, and the low-momentum region is populated by two multibody components: the $D^*\bar{D}\pi$ (dark red line) between 0 and 0.6 GeV/c, observed at 4170 MeV, and $D^*\bar{D}^*\pi$ (black line) between 0 and 0.4 GeV/c, which is not present at lower energy.

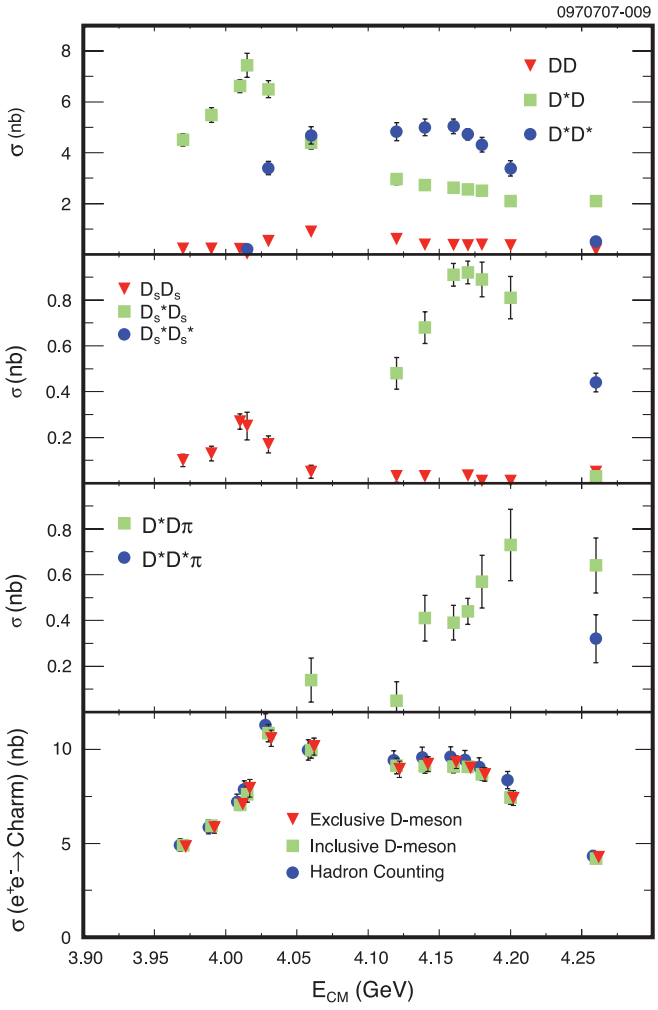

FIG. 6 (color). Exclusive cross sections for two-body and multibody charm-meson final states, and total observed charm cross section with combined statistical and systematic uncertainties.

TABLE III. Total systematic errors on the exclusive cross sections.

Mode	Relative error (10^{-2})
Determined by momentum fits	
$D\bar{D}$	4.5
$D\bar{D}^*$	3.4
$D^*\bar{D}^*$	4.7
$D^*\bar{D}\pi$	12.0
$D^*\bar{D}^*\pi$	25.0
Determined by counting	
$D_s^+D_s^-$	5.6
$D_s^+D_s^{*-}$	5.3
$D_s^{*+}D_s^{*-}$	6.8

selection, extraction of yields, and overall normalization. The total systematic uncertainty (Table III) is not dominated by any one of these.

Track selection and particle identification closely follow previous CLEO-c analyses [12,15]. The efficiency for reconstructing charged tracks has been estimated by a missing-mass technique applied to events collected at the $\psi(2S)$ and $\psi(3770)$ resonances. There is good agreement between data and the Monte Carlo simulation, with an estimated relative uncertainty of $\pm 0.7\%$ per track. Pion and kaon identification has been studied with D^0 and D^+ decays in $\psi(3770)$ data, with estimated systematic uncertainties in the respective efficiencies of $\pm 0.3\%$ and $\pm 1.3\%$. The uncertainties on reconstruction efficiencies for the neutral particles π^0 and η for D_s decays have been estimated at $\pm 2\%$ and $\pm 4\%$, respectively.

The extraction of event yields by fitting the charm-meson momentum spectra (non-D_s modes) incurs systematic uncertainty primarily through the signal functions obtained from Monte Carlo simulations, which depend on details of ISR and, in the case of $D^*\bar{D}^*$, the helicity amplitudes [18] and resulting D-meson angular distributions. As for the exclusive measurements, these details were studied with the large data sample at 4170 MeV, for which statistical uncertainties are small, and the resulting estimated relative systematic uncertainties are applied to all energy points. For the ISR calculation, the exclusive cross sections input to EVTGEN were varied from their nominal shapes. While a qualitative constraint of consistency with our measured cross sections was imposed, some extreme variations are included in the final systematic uncertainty. Both the direct effect on the fitted yield of varying a specific mode and the indirect effect of varying other modes were computed, although the former dominates in quadrature.

The yields for D_s final states are determined by direct counts after cutting on $M_{\rm bc}$ and ΔE. Systematic uncertainty arises in these measurements if the Monte Carlo simulation does not provide an accurate determination of the associated efficiency. This is probed by adjusting the selection criteria and recomputing the cross sections, again using the high-statistics sample at 4170 MeV. The systematic uncertainties assigned based on these studies are $\pm 3\%$, $\pm 2.5\%$ and $\pm 5\%$ for $D_s^+D_s^-$, $D_s^{*+}D_s^-$ and $D_s^{*+}D_s^{*-}$, respectively.

In converting the measured yields to cross sections we must correct for the branching fractions of the charm-meson decay modes. For each of the nonstrange charm mesons, only one mode is used and CLEO-c measurements [12] provide the branching fractions and uncertainties: $\pm 3.1\%$ for $D^0 \to K^-\pi^+$ and $\pm 3.9\%$ for $D^+ \to K^-\pi^+\pi^+$. For D_s modes we use CLEO-c measurements of the branching fractions for the eight decay modes included in the weighted sum [15]. The world-average value is used for the $D^{*+} \to D^0\pi^+$ branching fraction, with a systematic uncertainty of $\pm 0.7\%$ [5]. Finally, the cross-section normalization also depends on the absolute determination of the integrated luminosity for each data sample, with a systematic uncertainty of $\pm 1.0\%$ [13].

TABLE IV. Measured cross sections for final states consisting of two neutral nonstrange charm mesons. The first error on each cross section is statistical and the second is systematic.

$E_{\rm c.m.}$ (MeV)	$\sigma(D^0\bar{D}^0)$ (pb)	$\sigma(D^{*0}\bar{D}^0)$ (pb)	$\sigma(D^{*0}\bar{D}^{*0})$ (pb)
3970	$86 \pm 29 \pm 4$	$2280 \pm 134 \pm 78$	...
3990	$133 \pm 41 \pm 6$	$2740 \pm 157 \pm 93$	...
4010	$76 \pm 25 \pm 3$	$3320 \pm 13 \pm 113$	...
4015	<10 (90% C.L.)	$3840 \pm 283 \pm 131$	$213 \pm 76 \pm 9$
4030	$334 \pm 70 \pm 15$	$3200 \pm 183 \pm 109$	$2000 \pm 125 \pm 94$
4060	$410 \pm 72 \pm 18$	$2230 \pm 147 \pm 76$	$2290 \pm 132 \pm 108$
4120	$303 \pm 70 \pm 14$	$1400 \pm 135 \pm 48$	$2550 \pm 154 \pm 120$
4140	$177 \pm 40 \pm 8$	$1350 \pm 100 \pm 46$	$2443 \pm 116 \pm 115$
4160	$167 \pm 28 \pm 8$	$1252 \pm 69 \pm 43$	$2566 \pm 84 \pm 121$
4170	$177 \pm 7 \pm 8$	$1272 \pm 19 \pm 43$	$2363 \pm 19 \pm 111$
4180	$179 \pm 39 \pm 8$	$1211 \pm 92 \pm 41$	$2173 \pm 104 \pm 102$
4200	$180 \pm 55 \pm 8$	$1030 \pm 123 \pm 35$	$1830 \pm 139 \pm 86$
4260	$86 \pm 18 \pm 4$	$1080 \pm 59 \pm 37$	$269 \pm 42 \pm 13$

TABLE V. Measured cross sections for final states consisting of two charged nonstrange charm mesons. The first error on each cross section is statistical and the second is systematic.

$E_{\text{c.m.}}$ (MeV)	$\sigma(D^+\bar{D}^-)$ (pb)	$\sigma(D^{*+}\bar{D}^-)$ (pb)	$\sigma(D^{*+}\bar{D}^{*-})$ (pb)
3970	$137 \pm 26 \pm 6$	$2230 \pm 131 \pm 76$	···
3990	$90 \pm 22 \pm 4$	$2750 \pm 156 \pm 94$	···
4010	$135 \pm 22 \pm 6$	$3300 \pm 132 \pm 112$	···
4015	$38 \pm 20 \pm 2$	$3703 \pm 274 \pm 126$	···
4030	$196 \pm 35 \pm 9$	$3300 \pm 181 \pm 112$	$1400 \pm 170 \pm 66$
4060	$480 \pm 55 \pm 22$	$2170 \pm 143 \pm 74$	$2390 \pm 222 \pm 112$
4120	$310 \pm 50 \pm 14$	$1560 \pm 136 \pm 53$	$2280 \pm 232 \pm 107$
4140	$200 \pm 29 \pm 9$	$1376 \pm 98 \pm 47$	$2556 \pm 196 \pm 120$
4160	$200 \pm 21 \pm 9$	$1376 \pm 69 \pm 47$	$2479 \pm 135 \pm 117$
4170	$182 \pm 6 \pm 8$	$1285 \pm 18 \pm 44$	$2357 \pm 19 \pm 111$
4180	$197 \pm 27 \pm 9$	$1296 \pm 87 \pm 44$	$2145 \pm 172 \pm 101$
4200	$181 \pm 36 \pm 8$	$1070 \pm 116 \pm 36$	$1564 \pm 215 \pm 74$
4260	$94 \pm 13 \pm 4$	$1022 \pm 54 \pm 35$	$237 \pm 54 \pm 11$

TABLE VI. Measured cross sections for final states consisting of two strange charm mesons. The first error on each cross section is statistical and the second is systematic.

$E_{\text{c.m.}}$ (MeV)	$\sigma(D_s^+D_s^-)$ (pb)	$\sigma(D_s^{*+}D_s^-)$ (pb)	$\sigma(D_s^{*+}D_s^{*-})$ (pb)
3970	$102 \pm 26 \pm 6$	···	···
3990	$133 \pm 31 \pm 7$	···	···
4010	$269 \pm 30 \pm 15$	···	···
4015	$250 \pm 59 \pm 14$	···	···
4030	$174 \pm 36 \pm 10$	···	···
4060	$51 \pm 28 \pm 3$	···	···
4120	$26 \pm 26 \pm 1$	$478 \pm 64 \pm 25$	···
4140	$25 \pm 20 \pm 1$	$684 \pm 59 \pm 36$	···
4160	<15 (90% C.L.)	$905 \pm 11 \pm 48$	···
4170	$34 \pm 3 \pm 2$	$916 \pm 11 \pm 49$	···
4180	$7 \pm 16 \pm 1$	$889 \pm 59 \pm 47$	···
4200	$15 \pm 22 \pm 1$	$812 \pm 82 \pm 43$	···
4260	$47 \pm 22 \pm 3$	$34 \pm 9 \pm 2$	$440 \pm 27 \pm 30$

A mode-by-mode summary of the systematic uncertainties in the exclusive cross-section measurements is provided in Table III. The systematic errors are 100% correlated across energy.

TABLE VII. Measured cross sections for multibody final states, consisting of two charm mesons and an extra pion, for all data points above the production threshold. The first error on each cross section is statistical and the second is systematic.

$E_{\text{c.m.}}$ (MeV)	$\sigma(D^*\bar{D}\pi)$ (pb)	$\sigma(D^*\bar{D}^*\pi)$ (pb)
4060	$144 \pm 94 \pm 17$	···
4120	$45 \pm 83 \pm 5$	···
4140	$412 \pm 87 \pm 49$	···
4160	$389 \pm 60 \pm 47$	···
4170	$440 \pm 20 \pm 53$	···
4180	$575 \pm 92 \pm 69$	···
4200	$735 \pm 129 \pm 88$	···
4260	$638 \pm 93 \pm 77$	$322 \pm 67 \pm 80$

The cross-section measurements are presented in Tables IV, V, and VI (modes with only two charm mesons), and Table VII (multibody modes).

As a cross-check, for the two largest data samples (4170 and 4260 MeV), the multibody cross sections are also determined by fitting the distributions of missing mass against detected $D^0\pi$, $D^+\pi$ and $D^*\pi$ combinations. While these measurements are generally less precise, they show good agreement with the results of the momentum-spectrum fits. Details of this study are provided in Ref. [18].

VI. INCLUSIVE CROSS-SECTION MEASUREMENTS

If all final states have been included, the sum of the exclusive cross sections should equal the total charm cross section. We test this supposition with two inclusive measurements that can also be compared with past results.

The first cross-check is a measurement of the total charm-meson cross section:

$$\sigma(e^+e^- \to D\bar{D}X) = \frac{\sigma_{D^0} + \sigma_{D^+} + \sigma_{D_s^+}}{2}, \qquad (1)$$

where the contributing cross sections are defined by $\sigma_D = N_D/\epsilon B\mathcal{L}$, where ϵ and B are the efficiency and branching fraction for the decay mode used ($D^0 \to K^-\pi^+$, $D^+ \to K^-\pi^+\pi^+$, and $D_s^+ \to K^-K^+\pi^+$), $\mathcal{L}$ is the integrated luminosity, and N_D is the yield obtained by fitting the mass spectrum. In the case of D^0 and D^+, the invariant-mass distribution is fitted to a Gaussian signal and polynomial background. For D_s, the event-type requirements are maintained because of the relatively large background for the high-yield $K^-K^+\pi^+$ decay mode. For our energy points below 4120 MeV, where D_s production occurs only through $D_s^+D_s^-$, the yield is extracted by fitting $M_{\rm bc}$ to a Gaussian signal and ARGUS background function [19]. For 4120 MeV and above, event types involving D_s^{*+} contribute. For all candidate events that pass the selection requirements for any of $D_s^+D_s^-$, $D_s^{*+}D_s^-$, and $D_s^{*+}D_s^{*-}$ (the last only for 4260 MeV), a fit to the D_s^+ invariant mass is used to determine the yield.

The second cross-check is a determination of the total cross section made by counting multihadronic events. The contribution of uds continuum production is estimated with measurements made at $E_{\rm c.m.} = 3671$ MeV, below $c\bar{c}$ threshold, and extrapolated as $1/s$. Procedures for this measurement are identical to those used to determine the cross section for $e^+e^- \to \psi(3770) \to$ hadrons in CLEO-c data at $E_{\rm c.m.} = 3770$ MeV [20].

Figure 6 (bottom frame) shows the inclusive measurements (statistical and systematic uncertainties combined in quadrature) and the sum of the cross sections for the measured exclusive final states without radiative corrections. The excellent agreement demonstrates that, to current precision, the measured exclusive two- and three-body final states saturate charm production in this region. Furthermore, charm is demonstrated to account for all production of multihadronic events above the extrapolated uds cross section.

For the inclusive-charm cross-section measurements, the systematic uncertainties associated with the per-particle efficiencies for tracking and particle identification are identical to those of the exclusive measurements. The uncertainties in normalization (luminosity and branching fractions) are also identical. Systematic uncertainty in the yield extraction is dominated by the choice of fitting function. This is evaluated mode by mode and propagated into overall systematic uncertainties accounting for all correlations, with combined systematic uncertainties of $\pm 4.3\%$, $\pm 5.1\%$, and $\pm 8.6\%$ ($\pm$ 10.6%) for D^0, D^+, and D_s^+ below (above) 4120 MeV. For the hadron-counting inclusive cross sections, the systematic uncertainties are identical to those of Ref. [20]. The systematic errors for the hadron-counting method are slightly energy-dependent, varying between 5.2% and 6.1% due to the different amounts of J/ψ, $\psi(2S)$, and $\psi(3770)$ present at each energy.

Table VIII gives the inclusive cross sections and the sum of the exclusive cross sections with both statistical and systematic uncertainties.

For comparison with other experiments and theory it is necessary to obtain Born-level cross sections from the observed cross sections by correcting for ISR. We do this by calculating correction factors following the method of

TABLE VIII. Comparison of the total charm cross section determined by summing the exclusive measurements (Tables IV, VI, and VII) with those found by the two inclusive techniques: charm-meson counting and multihadronic-event counting. The first error on each measurement is statistical and the second systematic. The cross-section measurements are not radiatively corrected. The last column gives the value of R from the hadron-counting measurement, with radiative corrections as described in the text and correction for noncharm continuum production based on $R_{uds} = 2.285 \pm 0.03$, as determined by a $\frac{1}{s}$ fit to previous R measurements between 3.2 and 3.72 GeV [21].

Energy (MeV)	Exclusive D-meson (nb)	Inclusive D-meson (nb)	Hadron counting (nb)	R (ISR-corrected)
3970	$4.83 \pm 0.19 \pm 0.15$	$4.91 \pm 0.18 \pm 0.16$	$4.91 \pm 0.13 \pm 0.30$	$3.36 \pm 0.04 \pm 0.05$
3990	$5.85 \pm 0.23 \pm 0.19$	$5.93 \pm 0.21 \pm 0.19$	$5.87 \pm 0.14 \pm 0.34$	$3.55 \pm 0.05 \pm 0.06$
4010	$7.10 \pm 0.14 \pm 0.23$	$7.05 \pm 0.17 \pm 0.23$	$7.21 \pm 0.12 \pm 0.40$	$3.88 \pm 0.04 \pm 0.08$
4015	$7.94 \pm 0.41 \pm 0.26$	$7.62 \pm 0.34 \pm 0.25$	$7.88 \pm 0.18 \pm 0.43$	$3.95 \pm 0.08 \pm 0.08$
4030	$10.60 \pm 0.34 \pm 0.27$	$10.87 \pm 0.28 \pm 0.37$	$11.30 \pm 0.15 \pm 0.59$	$4.74 \pm 0.07 \pm 0.12$
4060	$10.16 \pm 0.36 \pm 0.27$	$9.98 \pm 0.26 \pm 0.34$	$9.98 \pm 0.14 \pm 0.53$	$4.34 \pm 0.05 \pm 0.10$
4120	$8.95 \pm 0.37 \pm 0.25$	$9.13 \pm 0.28 \pm 0.31$	$9.43 \pm 0.15 \pm 0.49$	$4.21 \pm 0.06 \pm 0.10$
4140	$9.22 \pm 0.29 \pm 0.26$	$9.11 \pm 0.22 \pm 0.30$	$9.58 \pm 0.24 \pm 0.50$	$4.18 \pm 0.04 \pm 0.10$
4160	$9.33 \pm 0.20 \pm 0.26$	$9.10 \pm 0.15 \pm 0.30$	$9.62 \pm 0.17 \pm 0.50$	$4.18 \pm 0.03 \pm 0.10$
4170	$9.03 \pm 0.04 \pm 0.25$	$9.09 \pm 0.07 \pm 0.30$	$9.45 \pm 0.09 \pm 0.49$	$4.20 \pm 0.01 \pm 0.10$
4180	$8.67 \pm 0.27 \pm 0.24$	$8.70 \pm 0.20 \pm 0.29$	$9.07 \pm 0.12 \pm 0.47$	$4.17 \pm 0.04 \pm 0.10$
4200	$7.42 \pm 0.35 \pm 0.20$	$7.45 \pm 0.26 \pm 0.25$	$8.37 \pm 0.14 \pm 0.43$	$3.77 \pm 0.05 \pm 0.08$
4260	$4.27 \pm 0.16 \pm 0.14$	$4.20 \pm 0.10 \pm 0.14$	$4.34 \pm 0.16 \pm 0.23$	$3.06 \pm 0.02 \pm 0.04$

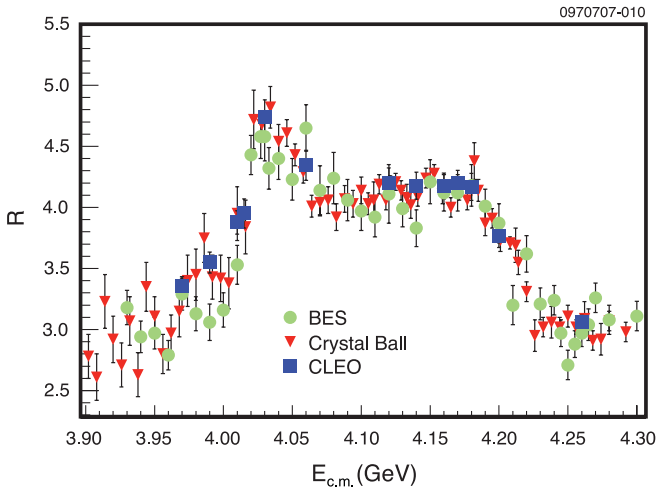

FIG. 7 (color). R (including radiative corrections) from this analysis and from previous measurements [6,21].

Kuraev and Fadin [22], which is augmented with the explicit addition of the effect of vacuum polarization, including μ and τ loops. The observed cross section at any $\sqrt{s}$ is then given by

$$\sigma_{\rm obs}(s) = \int_0^1 dk \cdot f(k,s)\sigma_B(s_{\rm eff}), \qquad (2)$$

where the Born cross section σ_B is a function of the effective center-of-mass energy squared $[k = (s - s_{\rm eff})/s]$, and $f(k,s)$ is the ISR kernel. The radiative-correction factor is also calculated following the alternative implementation of Bonneau and Martin [23], which includes vacuum polarization. The differences between the two methods have been verified to be small, and we take the difference between them as an estimate of the theoretical uncertainty in the calculation of the radiative-correction factor. We also consider the larger systematic uncertainty due to our approximation of $\sigma_B(s_{\rm eff})$, required for Eq. (2), by taking the difference between a simple linear interpolation and a fit to a sum of Breit-Wigner functions to both the BES [6] and Crystal Ball (CB) [21] R measurements. Figure 7 shows that there is excellent agreement between our inclusive-charm measurement and the previous R measurements.

VII. SUMMARY AND CONCLUSIONS

In summary, we have presented detailed information about charm production above $c\bar{c}$ threshold. Realizing the main objective of the CLEO-c scan run, we find the center-of-mass energy that maximizes the yield of D_s to be 4170 MeV, where the cross section of $\sim$0.9 nb is dominantly $D_s^{*+}D_s^-$. This information has guided the planning of subsequent CLEO-c running, with initial results already presented on leptonic [24] and hadronic [15] D_s decays.

The total charm cross section between 3.97 and 4.26 GeV has been measured both inclusively and exclusively by summing over two-body and multibody final states. The multibody signal has not previously been observed and its detailed composition has not been determined. Momentum and recoil-mass distributions are consistent with dominance by the nonresonant final states $D\bar{D}^*\pi$ and $D^*\bar{D}^*\pi$, but it could also include two-body decays with higher excitations $D_J^{(*)}$ that decay into $D^{(*)}\pi$. Analysis of the detailed composition of these states, for example through measurements of D angular distributions, would require a much larger data sample than we currently have available.

The consistency of our charm cross-section measurements is excellent, and radiatively corrected inclusive cross sections are consistent with previous experimental results. Figure 6 shows that the observed exclusive cross sections for $D\bar{D}$, $D^*\bar{D}$, $D^*\bar{D}^*$, $D_s^+D_s^-$, $D_s^{*+}D_s^-$, $D_s^{*+}D_s^{*-}$, $D^*\bar{D}\pi$, and $D^*\bar{D}^*\pi$ exhibit structure that reflects the intricate behavior expected in the charm-threshold region. Figure 8 provides a comparison between our measured cross sections and the updated calculation of Eichten *et al.* [9,25]. There is reasonable qualitative agreement for most of the two-charm-meson final states. The most

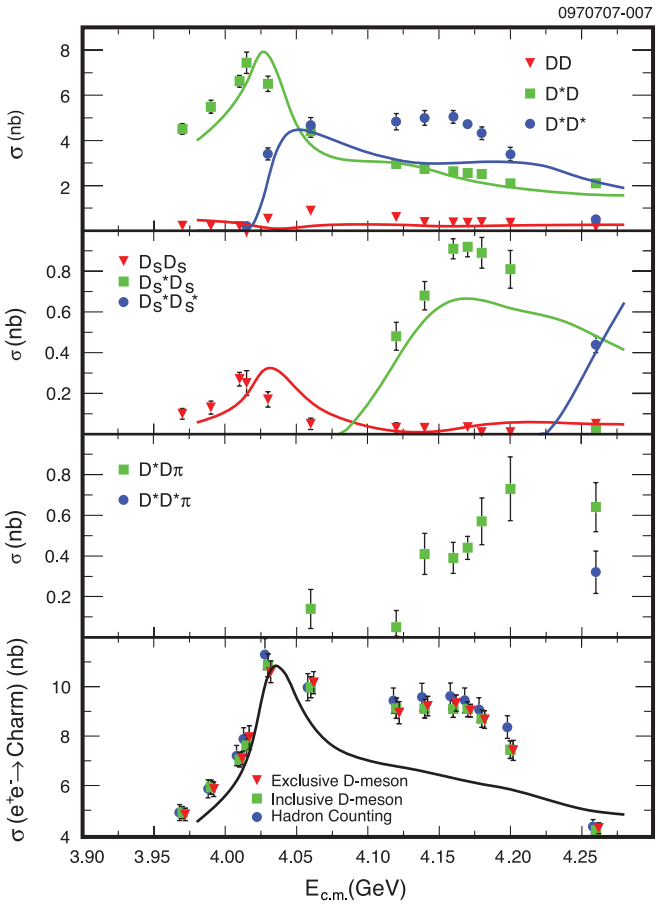

FIG. 8 (color). Comparisons between measured cross sections and the updated predictions of the potential model of Eichten *et al.* [9,25] (solid lines).

notable exception is the cross section for $D^*\bar{D}^*$ in the region between 4050 and 4200 MeV, where the measurement exceeds the prediction by as much as 2 nb. This corresponds to nearly a factor-of-two disagreement in the ratio of $D^*\bar{D}^*$ to $D^*\bar{D}$ production, accounting for about two thirds of the difference in the total charm cross section. This is a much larger effect than the absence of a multibody component from the theoretical prediction.

It has been suggested by Dubynskiy and Voloshin [26] that the existence of a peak in the $D^*\bar{D}$ and $D_s^+D_s^-$ channels at the $D^*\bar{D}^*$ threshold, along with the observation that there is a minimum in $D\bar{D}$, in agreement with recent results from *BABAR* [27], can be interpreted as a possible new narrow resonance, but available data are insufficient for a definitive assessment.

The $D^*\bar{D}^*$ cross section exhibits a plateau just above its threshold. This contrasts with $D^*\bar{D}$, which we observe to peak at threshold, in agreement with recent results from Belle [28].

Studies of open-charm production at 4260 MeV have the potential to discriminate among possible explanations of the nature of the $Y(4260)$. For example, hybrid charmonium models predict a large coupling to the wide $D_1(2430)^0\bar{D}^0$ and a small one to $D_s^+D_s^-$ [29]. A tetraquark interpretation suggests a large decay to $D\bar{D}$ or $D_s^+D_s^-$ [29–31]. Complicated threshold effects could lead to enhancement of the $D^*\pi$ final state through off shell production of D_1 [32]. Tables IV, VI, and VII show no evidence for enhancement of the cross section for any open-charm final states at 4260 MeV. CLEO-c has previously confirmed the $Y(4260)$ through its decay to $\pi^+\pi^-J/\psi$, measuring $\sigma(\pi^+\pi^-J/\psi) = 58^{+12}_{-10} \pm 4$ pb [2]. Under the assumption that all open-charm production is accounted for by $Y(4260)$ decays, it is possible to set conservative upper limits on the ratio of the cross section for production of $Y(4260)$ and decay to our measured open-charm states to that for production and decay to $\pi^+\pi^-J/\psi$. Table IX provides a compilation of these limits. The lack of obvious enhancement in any open-charm channel relative to other energies, which is in stark contrast to the clear enhancement in $\pi^+\pi^-J/\psi$, tends to disfavor the hybrid charmonium and tetraquark proposals. More definitive statements will require additional data from future experiments.

TABLE IX. Upper limits (90% confidence level) on the ratio of the cross section for production of $Y(4260)$ and decay to our measured open-charm states at 4260 MeV to that for production of $Y(4260)$ and decay to $\pi^+\pi^-J/\psi$.

Final state (X)	$\frac{\sigma(Y(4260)\to X)}{\sigma(Y(4260)\to\pi^+\pi^-J/\psi)}$
$D\bar{D}$	<4.0
$D^*\bar{D}$	<45
$D^*\bar{D}^*$	<11
$D^*\bar{D}\pi$	<15
$D^*\bar{D}^*\pi$	<8.2
$D_s^+D_s^-$	<1.3
$D_s^{*+}D_s^-$	<0.8
$D_s^{*+}D_s^{*-}$	<9.5

ACKNOWLEDGMENTS

We gratefully acknowledge the effort of the CESR staff in providing us with excellent luminosity and running conditions. We thank E. Eichten and M. Voloshin for useful discussions. D. Cronin-Hennessy and A. Ryd thank the A. P. Sloan Foundation. This work was supported by the National Science Foundation, the U.S. Department of Energy, the Natural Sciences and Engineering Research Council of Canada, and the U.K. Science and Technology Facilities Council.

[1] B. Aubert *et al.* (*BABAR* Collaboration), Phys. Rev. Lett. **95**, 142001 (2005).
[2] T. E. Coan *et al.* (CLEO Collaboration), Phys. Rev. Lett. **96**, 162003 (2006).
[3] C. Z. Yuan *et al.* (Belle Collaboration), Phys. Rev. Lett. **99**, 182004 (2007).
[4] M. Kobayashi and T. Maskawa, Prog. Theor. Phys. **49**, 652 (1973).
[5] S. Eidelman *et al.* (Particle Data Group), Phys. Lett. B **592**, 1 (2004).
[6] J. Z. Bai *et al.* (BES Collaboration), Phys. Rev. Lett. **88**, 101802 (2002).
[7] T. Barnes, J. Phys. Conf. Ser. **9**, 127 (2005).
[8] T. Barnes, arXiv:hep-ph/0406327.
[9] E. Eichten, K. Gottfried, T. Kinoshita, K. D. Lane, and T. M. Yan, Phys. Rev. D **21**, 203 (1980).
[10] M. B. Voloshin, arXiv:hep-ph/0602233.
[11] R. A. Briere *et al.* (CESR-c, CLEO-c Taskforces, and CLEO-c Collaboration), Cornell University, LEPP Report No. CLNS 01/1742, 2001 (unpublished).
[12] Q. He *et al.* (CLEO Collaboration), Phys. Rev. Lett. **95**, 121801 (2005); **96**, 199903 (2006).
[13] S. Dobbs *et al.* (CLEO Collaboration), Phys. Rev. D **76**, 112001 (2007).
[14] Y. Kubota *et al.* (CLEO Collaboration), Nucl. Instrum. Methods Phys. Res., Sect. A **320**, 66 (1992); M. Artuso *et al.*, *ibid.* **554**, 147 (2005); D. Peterson *et al.*, *ibid.* **478**, 142 (2002).

[15] J. Alexander *et al.* (CLEO Collaboration), Phys. Rev. Lett. **100**, 161804 (2008).
[16] R. Brun *et al.*, GEANT 3.21, CERN Program Library Long Writeup W5013, 1993 (unpublished).
[17] D. J. Lange, Nucl. Instrum. Methods Phys. Res., Sect. A **462**, 152 (2001).
[18] B. W. Lang, Ph.D. thesis, University of Minnesota [arXiv:0801.1092v1].
[19] H. Albrecht *et al.* (ARGUS Collaboration), Phys. Lett. B **241**, 278 (1990).
[20] D. Besson *et al.* (CLEO Collaboration), Phys. Rev. Lett. **96**, 092002 (2006).
[21] A. Osterheld *et al.*, SLAC Report No. SLAC-PUB-4160, 1986.
[22] E. A. Kuraev and V. S. Fadin, Yad. Fiz. **41**, 733 (1985) [Sov. J. Nucl. Phys. **41**, 466 (1985)].
[23] G. Bonneau and F. Martin, Nucl. Phys. **B27**, 381 (1971).
[24] M. Artuso *et al.* (CLEO Collaboration), Phys. Rev. Lett. **99**, 071802 (2007).
[25] E. Eichten, in Proceedings of the International Workshop on Heavy Quarkonium, Brookhaven National Laboratory, 2006 (unpublished); private communication.
[26] S. Dubynskiy and M. B. Voloshin, Mod. Phys. Lett. A **21**, 2779 (2006).
[27] B. Aubert *et al.* (*BABAR* Collaboration), Phys. Rev. D **76**, 111105 (2007).
[28] K. Abe *et al.* (Belle Collaboration), Phys. Rev. D **77**, 011103 (2008); G. Pakhlova *et al.* (Belle Collaboration), Phys. Rev. Lett. **98**, 092001 (2007).
[29] F. E. Close and P. R. Page, Phys. Lett. B **628**, 215 (2005).
[30] D. Ebert, R. N. Faustov, and V. O. Galkin, Phys. Lett. B **634**, 214 (2006).
[31] L. Maiani, V. Riquer, F. Piccinini, and A. D. Polosa, Phys. Rev. D **72**, 031502(R) (2005).
[32] J. L. Rosner, Phys. Rev. D **74**, 076006 (2006).